Design Optimization of Short-Stroke Single-Phase Tubular Permanent-Magnet Motor for Refrigeration Applications

Jiabin Wang, *Senior Member, IEEE*, David Howe, and Zhengyu Lin, *Member, IEEE*

***Abstract*—This paper describes a design methodology to achieve optimal performance for a short-stroke single-phase tubular permanent-magnet motor which drives a reciprocating vapor compressor. The steady-state characteristic of the direct-drive linear-motor compressor system is analyzed, an analytical formula for predicting iron loss is presented, and a motor-design procedure which takes into account the effect of compressor loads under nominal operating condition is formulated. It is shown that the motor efficiency can be optimized with respect to two leading dimensional ratios. Experimental results validate the proposed design methodology.**

***Index Terms*—Linear machines, permanent-magnet (PM) machines, reciprocating compressors.**

NOMENCLATURE

A_e	Effective coil area in square meters.
B	Viscous-damping coefficient in newton-seconds per meter.
B_m	Peak flux density in tesla.
B_r	Remanence of permanent magnets (PMs) in tesla.
b_0	Width of slot opening in meters.
f	Electrical frequency in hertz.
f_0	Resonant frequency in hertz.
G	Air-gap length in meters.
$h_{\rm eq}$	Equivalent hysteretic damping coefficient of compressed-gas force in newtons per meter.
h_m	Radial thickness of magnets in meters.
h_t	Tooth-tip height in meters.
$h_{\rm ym}$	Radial thickness of supporting tube in meters.
$h_{\rm ys}$	Yoke thickness of stator core in meters.
$\dot{I}$	Current phasor in amperes.
$J_{\rm rms}$	Rms current density in amperes per square meter.
K	Total stiffness of tuned suspension spring in newtons per meter.
$K_{\rm FPT}$	Average motor force coefficient per turn in newtons per ampere.
$K_{\rm Ta}$	Average motor force coefficient in newtons per ampere.
$k_{\rm eq}$	Equivalent stiffness of compressed-gas force in newtons per meter.
k_h	Hysteresis iron-loss-density coefficient.
L	Motor inductance in henry.
$L_{\rm es}$	Equivalent inductance of compressor system in henry.
$L_{\rm ec}$	Equivalent inductance of mechanical and gas-compression cycle in henry.
L_{s0}	Motor inductance per turn in henry.
l_e	Average radius of coil per turn in meters.
m	Total moving mass in kilograms.
N_c	Number of turns of coil.
$P_{\rm cu}$	Motor copper loss in watts.
P_e	Excess iron-loss component in watts.
P_h	Hysteresis iron-loss component in watts.
$P_{\rm in}$	Motor input power in watts.
P_f	Coil packing factor.
$P_{\rm fe}$	Motor iron loss in watts.
$P_{\rm out}$	Motor output power in watts.
p_e	Excess iron-loss density in watts per kilogram.
p_h	Hysteresis iron-loss density in watts per kilogram.
R	Motor resistance in ohms
R_e	Outer radius of stator in meters.
$R_{\rm ec}$	Equivalent resistance of mechanical and gas-compression cycle in ohms.
$R_{\rm ep}$	Equivalent resistance of gas-compression cycle in ohms.
$R_{\rm ev}$	Equivalent resistance of viscous damping in ohms.
$R_{\rm es}$	Equivalent resistance of compressor system in ohms.
R_i	Inner radius of supporting tube in meters.
R_m	Outer radius of magnets in meters.
$T_{\rm mr}$	Axial length of radially magnetized magnet at the center in meters.
$T_{\rm mr2}$	Axial length of radially magnetized magnets at two ends in meters.
$T_{\rm mz}$	Axial length of axially magnetized magnets in meters.
T_p	Pole pitch in meters.
$T_{\rm pe}$	Extended tooth-tip length in meters.
$T_{\rm pw}$	Tooth-pitch width in meters.
T_w	Tooth width in meters.
$\dot{U}$	Piston-amplitude phasor in meters.
$\dot{V}$	Supply-voltage phasor in volts.
$V_{\rm rms}$	Rms supply voltage in volts.
$Z_{\rm es}$	Equivalent impedance of compressor system in ohms.
α	Stator under cut angle in radians.
δ	Hysteresis iron-loss-density coefficient.

Manuscript received January 27, 2009; revised June 12, 2009. First published June 19, 2009; current version published December 11, 2009.

The authors are with the Electrical Machines and Drives Research Group, Department of Electrical and Electronic Engineering, The University of Sheffield, Sheffield, S1 3JD, U.K. (e-mail: j.b.wang@sheffield.ac.uk).

Color versions of one or more of the figures in this paper are available online at http://ieeexplore.ieee.org.

Digital Object Identifier 10.1109/TIE.2009.2025710

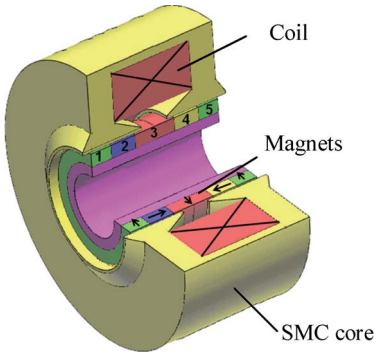

Fig. 1. Schematic of short-stroke single-phase tubular PM motor.

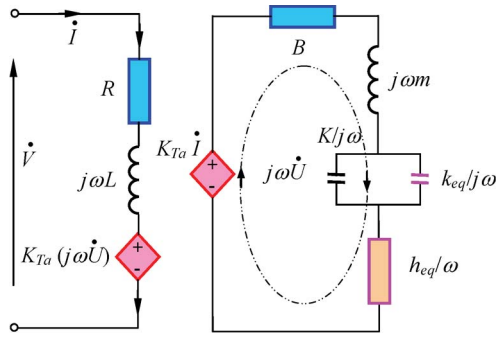

Fig. 2. Electrical equivalent circuit of linear compressor.

φ Power factor angle in radians.
ρ Resistivity of copper wire in ohms per meter.
θ_e Electrical angle in radians.
ω Electrical angular frequency in radians per second.

I. Introduction

In conventional refrigerator compressors, a rotary electrical motor (usually induction motor) drives a reciprocating pump through a crank. The overall efficiency of the system is relatively low, due to the inherent low efficiency of induction motors and the mechanical friction which is associated with the crank-driven piston. A reciprocating compressor driven by a linear motor [1]–[4] eliminates the side force on the cylinder wall caused by the crank shaft and therefore not only significantly reduces the frictional loss but also provides a simple means for modulating the refrigerator load according to the demand and results in additional energy saving.

There are various linear-machine technologies and numerous topologies which might be employed in reciprocating linear-compressor applications [5], [6]. The main technologies are induction machines, PM machines [7]–[12], and switched-reluctance machines [13], [14]. Of the possible topologies, tubular configurations are compatible with the packaging/integration requirements of vapor compressors—since they have zero net radial force between the armature and stator, no end windings, and are volumetrically efficient [6], [7], [15]. However, due to their significantly higher efficiency, only PM-excited machines are deemed to be appropriate for the proposed compressor applications [6].

A novel short stroke single-phase tubular PM motor, as shown in Fig. 1, for linear compressor applications has been reported and its performance analyzed [16], [17]. It employs a two-pole quasi-Halbach magnetized armature, having radially magnetized ring magnets placed at the center and both ends, and a soft magnetic composite (SMC) stator core which carries a single-phase coil. Such a coil is easy to manufacture and results in a very high packing factor, which is conducive to high efficiency [18]. The quasi-Halbach magnetized armature generates a magnetic field which is linked with the single-phase stator coil. Reciprocating thrust force is produced as a result of the interaction between the permanent magnetic field and the stator current when it is synchronized with the armature movement. Since the linear motor is directly coupled to the compressor load, it is essential that the design optimization takes into account the steady-state characteristics of the compressor operation.

II. Steady-State Performance of Linear-Motor Compressor System

It has been shown [19], [20] that due to the low-pass-filter effect of the mechanical mass-spring-damper subsystem, the piston velocity and the displacement of the compressor vary essentially sinusoidally with time, and higher order harmonics can be neglected. Thus, the steady-state behavior of the linear compressor system is governed by

$$\begin{aligned}\left[(K+k_{\rm eq}-\omega^2 m)+j(\omega B+h_{\rm eq})\right]\dot{U}&=K_{\rm Ta}\dot{I}\\ jK_{\rm Ta}\omega\dot{U}+(j\omega L+R)\dot{I}&=\dot{V}\end{aligned}\tag{1}$$

where ω is the angular frequency of the supply, $\dot{U}$, $\dot{I}$, and $\dot{V}$ represent the piston-amplitude phasor and the motor-current and voltage phasors, respectively, $K_{\rm Ta}$ is the average value of the force or back-EMF coefficient [6] of the linear motor over the piston stroke, and $k_{\rm eq}$ and $h_{\rm eq}$ are the equivalent stiffness and hysteretic damping coefficient of the gas force, respectively [19]. K is the total stiffness of the tuned suspension springs, B is the viscous-damping coefficient that represents the frictional effect between the cylinder and piston, and m is the total moving mass. L and R are the inductance and resistance of the linear motor, respectively. Using the analogy between mechanical and electrical quantities, (1) can be represented by the electrical equivalent circuit shown in Fig. 2, in which the displacement phasor $\dot{U}$ is analogous to the electric-charge phasor and $j\omega\dot{U}$ is the equivalent current phasor. Thus, the mass is equivalent to an inductor, whereas the spring is analogous to a capacitor. The power dissipated in the equivalent resistance $h_{\rm eq}/\omega$ represents the effective work which is done on the gas compression. The interaction between the electrical and mechanical systems is represented by the two current-controlled voltage sources.

Solving for $\dot{I}$ yields

$$\dot{I}=\frac{\dot{V}}{Z_{\rm es}}=\frac{\dot{V}}{R_{\rm es}+j\omega L_{\rm es}}=\frac{V}{|Z_{\rm es}|}\angle\varphi\tag{2}$$

where $Z_{\rm es}$, $R_{\rm es}$, and $L_{\rm es}$ are the equivalent impedance, resistance, and inductance of the linear compressor system,

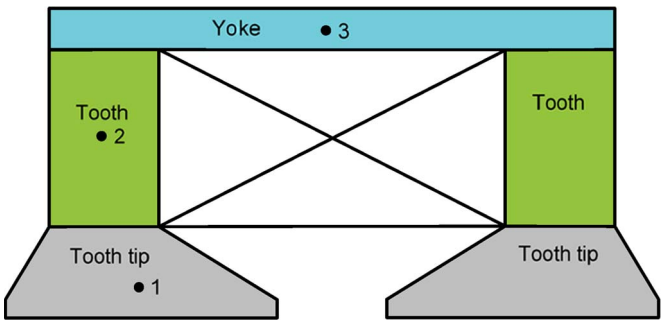

Fig. 3. Schematic of stator core.

respectively, and are given by

$$\begin{aligned} R_{\rm es} &= R + R_{\rm ec} \qquad L_{\rm es} = L + L_{\rm ec} \\ R_{\rm ec} &= \omega K_{\rm Ta}^2 (\omega B + h_{\rm eq})/\Delta \\ L_{\rm ec} &= K_{\rm Ta}^2 (K + k_{\rm eq} - \omega^2 m)/\Delta \\ \Delta &= (K + k_{\rm eq} - \omega^2 m)^2 + (\omega B + h_{\rm eq})^2. \end{aligned} \tag{3}$$

The equivalent resistance $R_{\rm ec}$ representing the mechanical system and gas-compression cycle can be separated into the viscous-damping component $R_{\rm ev}$ and compressor-work component $R_{\rm ep}$, i.e.,

$$\begin{aligned} R_{\rm ec} &= R_{\rm ev} + R_{\rm ep} \\ R_{\rm ev} &= \omega^2 K_{\rm Ta}^2 B/\Delta \\ R_{\rm ep} &= \omega K_{\rm Ta}^2 h_{\rm eq}/\Delta. \end{aligned} \tag{4}$$

The input and output powers $P_{\rm in}$ and $P_{\rm out}$, the efficiency η, and the power factor $\cos\varphi$ of the system can therefore be calculated from

$$\begin{aligned} \cos\varphi &= \frac{R_{\rm es}}{\sqrt{R_{\rm es}^2 + (\omega L_{\rm es})^2}} \\ P_{\rm in} &= VI\cos\varphi + P_{\rm fe} \\ P_{\rm out} &= R_{\rm ep} I^2 \\ \eta &= \frac{P_{\rm out}}{P_{\rm in}} = \frac{R_{\rm ep} I^2}{VI\cos\varphi + P_{\rm fe}} \end{aligned} \tag{5}$$

where $P_{\rm fe}$ is the iron loss of the motor and can be predicted analytically or by finite element (FE) analysis [20]. It can be shown [19] that the system operates most efficiently at the resonant frequency $f_0 = \sqrt{(k_{\rm eq} + K)/m}/(2\pi)$. It is evident that operating conditions of the compressor will affect the input impedance of the electrical system.

III. Iron-Loss Calculation

An analytical method for predicting iron loss $P_{\rm fe}$ in the short-stroke single-phase tubular PM motor has been established. The stator core is divided into three regions, namely, tooth, tooth tip, and yoke, as shown in Fig. 3.

The prediction is based on the flux-density waveforms for each region being analytically determined [16]. The total iron loss is given by

$$P_{\rm fe} = \sum_{i=m} (P_{\rm hi} + P_{\rm ci} + P_{\rm ei}). \tag{6}$$

$P_{\rm hi}$, $P_{\rm ci}$, and $P_{\rm ei}$ are the hysteresis loss, the classical eddy-current loss and excess eddy-current loss in the ith region, respectively. For SMC materials, the classical eddy-current loss component P_c is negligible due to the conductivity of the material that is virtually zero. However, the excess eddy-current loss component which is associated with domain-wall effects may still exist. Using analytically predicted flux-density waveforms [16], the hysteresis and excess loss densities in each region can be evaluated by

$$p_h = k_h f B_m^{\delta} \tag{7}$$

$$p_e = \sqrt{2\pi} f^{\frac{3}{2}} \int_{2\pi} \left| \frac{dB_s}{d\theta_e} \right|^{\frac{3}{2}} d\theta_e \tag{8}$$

where f, B_m, and θ_e are the frequency, the peak flux density, and electrical angle, respectively. B_s is the flux density of the region. The coefficients δ and k_h associated with the hysteresis loss component are determined from the manufacturer's data sheet.

IV. Number of Coil Turns

Equation (2) can be used to determine the number of coil turns for a given rms supply voltage $V_{\rm rms}$ under nominal operating conditions. The rms value of the motor current I can be expressed in terms of the rms current density $J_{\rm rms}$, the packing factor P_f, the number of coil turns N_c, and the effective coil area A_e

$$I = J_{\rm rms} A_e P_f / N_c. \tag{9}$$

The resistance of the coil is given by

$$R = (2\pi l_e \rho / P_f A_e) N_c^2 \tag{10}$$

where l_e is the average radius of the coil per turn and ρ is the resistivity of the copper wire. Thus, the voltage across the equivalent resistance can be expressed as

$$\begin{aligned} I(R + R_{\rm ec}) &= (K_{\rm re} + K_{\rm rec}) N_c \\ K_{\rm re} &= 2\pi l_e \rho J_{\rm rms} \\ K_{\rm rec} &= \omega J_{\rm rms} A_e P_f K_{\rm FPT}^2 (\omega B + h_{\rm eq})/\Delta \end{aligned} \tag{11}$$

where $K_{\rm FPT} = K_{\rm Ta}/N_c$ is the average motor-force coefficient per turn. Similarly, the inductance of the motor is proportional to the square of the coil turn N_c

$$L = L_{s0} N_c^2 \tag{12}$$

where L_{s0} is the inductance per turn. The voltage across the equivalent inductance is written as

$$\begin{aligned} I\omega(L + L_{\rm ec}) &= (K_{\rm le} + K_{\rm lec}) N_c \\ K_{\rm le} &= \omega L_{s0} J_{\rm rms} A_e P_f \\ K_{\rm lec} &= \omega J_{\rm rms} A_e P_f K_{\rm FPT}^2 (K + k_{\rm eq} - m\omega^2)/\Delta. \end{aligned} \tag{13}$$

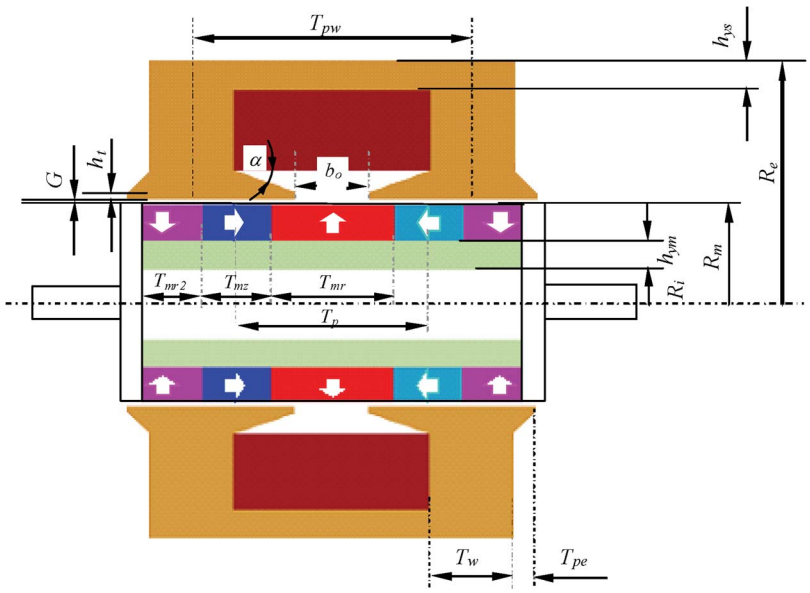

Fig. 4. Schematic and design parameters of linear motor.

For a given value of permissible rms current density $J_{\rm rms}$ which is dependent on the operating condition of the motor, the number of coil turns can be obtained from (2) and is given by

$$N_c \le V_{\rm rms}/\sqrt{(K_{\rm re}+K_{\rm rec})^2+(K_{\rm le}+K_{\rm lec})^2}. \qquad (14)$$

As is evident, the number of coil turns N_c is strongly influenced by the compressor operating conditions as well as the motor-design parameters. Thus, it is essential that the steady-state operational behavior of the compressor is taken into account in the motor design optimization.

V. Design Optimization

An analytical framework for predicting the open-loop magnetic-field distribution, back EMF, and thrust force of the short-stroke single-phase tubular PM motor has been established and validated in [16], [17]. This, together with the performance and iron-loss predictions described in Sections II and III, has been used to study the influence of leading design parameters on the motor and compressor-system efficiency. For a given set of design and operating conditions, the number of coil turns is determined using (14).

Fig. 4 shows the schematic and design parameters of the linear motor. The relevant variables and symbols are defined in the nomenclature. In the 16 design parameters, h_t, b_0, and α have insignificant influence on the machine performance, and, therefore, their values are fixed to 0.001 m, 0.008 m, and 20°, respectively. Although the force capability of the motor increases as the air-gap length G decreases, its minimum value is limited by the manufacturing and assembly tolerances. In this design, the air-gap length G is fixed to 0.0008 m. The motor efficiency improves as the outer stator radius R_e increases. However, an initial design scan shows that for the given design specification, the efficiency improvement diminishes when R_e is greater than 0.050 m. Hence, this value is chosen for the outer stator radius R_e.

TABLE I
Design Specification

Supply voltage (Vrms)	230
Electrical supply frequency (Hz)	50
Rated stroke (mm)	10.5
Rated output power (W)	87

The leading design parameters which have significant influences on the machine performance are the dimension ratios R_m/R_e and $T_{\rm mr}/T_p$, and they are optimized in the subsequent design processes. In addition, the influence of the magnet thickness h_m, tooth-pitch width $T_{\rm pw}$, and the properties of soft and PM materials on the motor performance are also investigated. The tooth width T_w, the stator yoke thickness $h_{\rm ys}$, and the radial thickness of the mover back iron $h_{\rm ym}$ are dependent on given flux-density levels in these regions, and their values are determined during a design process. The effect of magnetic saturation in the stator core and mover back iron is accounted for by introducing a fictitious airgap [15] which incurs an MMF drop equivalent to that in the stator and mover irons. This value is iteratively adjusted against the nonlinear B–H curve of the materials until converging to an equilibrium point. It should be noted that in this particular application, the power and thrust-force capability of the machine is essentially limited by the efficiency requirement rather than by thermal constraints. Thus, a nominal motor operating temperature of 80 °C based on existing compressor products was used in the design process.

A. Influence of R_m/R_e and $T_{\rm mr}/T_p$

The influence of R_m/R_e and $T_{\rm mr}/T_p$ on the motor and compressor-system performance is investigated against the design specification given in Table I and with fixed values of

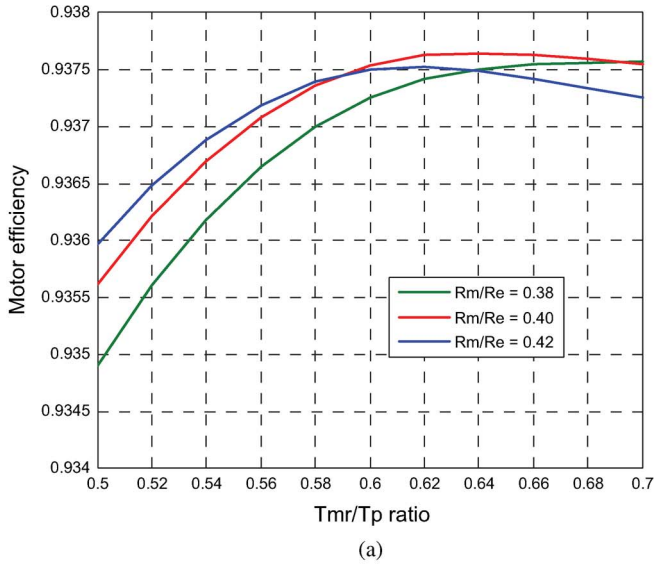

(a)

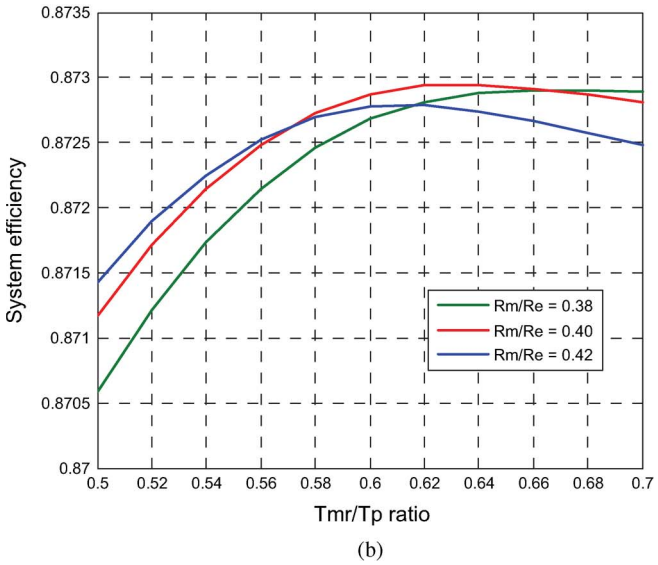

(b)

Fig. 5. Influence of R_m/R_e and $T_{\rm mr}/T_p$ on efficiency. (a) Motor efficiency. (b) System efficiency.

$h_m = 0.005$ m and $T_{\rm pw} = 0.04$ m and using sintered NdFeB magnets with $B_r = 1.04$ T and Somaloy 500 SMC [22] for the stator core.

Fig. 5 shows the variations of the motor efficiency and compressor-system efficiency with the 2-D ratios when the motor drives a typical compressor for household refrigerators. The compressor-system efficiency is calculated by dividing the power consumption on compressing R600a refrigerant by the electrical input power. As will be seen, there are optimal ratios of $T_{\rm mr}/T_p = 0.64$, $R_m/R_e = 0.40$, which yields the maximum motor efficiency of 0.938. It is evident that the optimal ratios of $T_{\rm mr}/T_p$ and R_m/R_e for the maximum system efficiency virtually coincide with the values for the maximum motor efficiency, albeit the $T_{\rm mr}/T_p$ ratio is slightly lower. The R_m/R_e ratio represents an optimal balance between electrical and magnetic loadings under the given volumetric and thermal constraints, whereas the $T_{\rm mr}/T_p$ ratio results in a maximum coil flux linkage produced by the two-pole quasi-Halbach magnetized magnets.

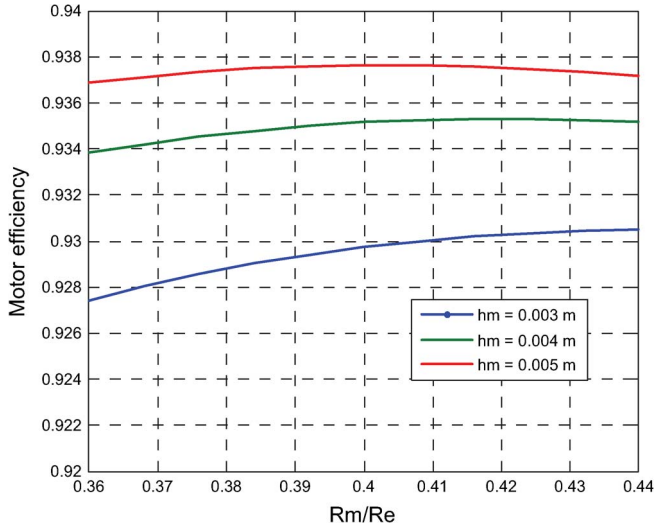

Fig. 6. Influence of h_m on motor efficiency.

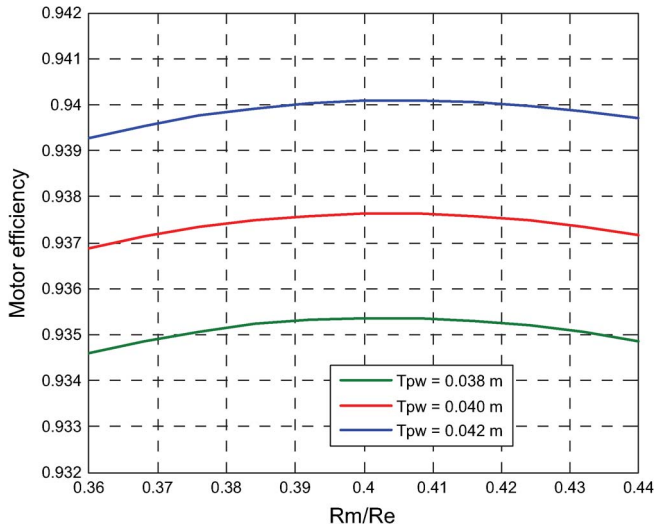

Fig. 7. Influence of tooth-pitch width on motor efficiency.

B. *Influence of* h_m

Fig. 6 shows the variations of the motor efficiency with the magnet thickness h_m and R_m/R_e, at the optimal ratio of $T_{\rm mr}/T_p = 0.62$, and with the other parameters being the same as previously stated. Similar variations of the compressor-system efficiency to that of the motor efficiency is observed but not plotted. It is evident that the motor efficiency increases as h_m increases. However, the improvement in efficiency diminishes when h_m is increased to greater than 0.005 m, while the weight and cost of the moving-magnet armature and the spring stiffness required for resonant operation become greater, which results in a less cost-effective solution. Hence, $h_m = 0.005$ m is appropriate for the radial thickness of the magnets.

C. *Influence of Tooth-Pitch Width* $T_{\rm pw}$

Fig. 7 shows the variations of the motor efficiency with the tooth-pitch width $T_{\rm pw}$ and R_m/R_e, for a fixed value of $h_m = 0.005$ m, and with the other parameters being the same as stated in Section V-B. As will be seen, as $T_{\rm pw}$ increases,

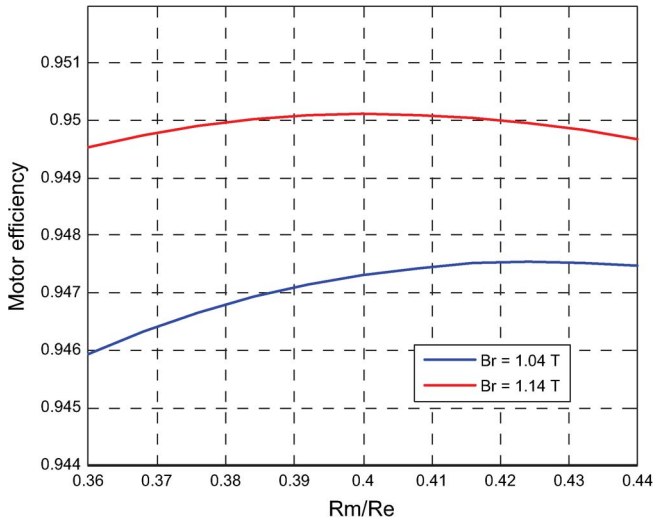

Fig. 8. Influence of B_r on motor efficiency.

the system performance continues to improve, although the rate of improvement is relatively small. The increase in $T_{\rm pw}$, however, gives rise to a large motor size and, hence, great cost. Considering the overall system dimensions and cost, a tooth-pitch width $T_{\rm pw} = 0.04$ m is selected. It is also evident that the optimal ratios R_m/R_e for the maximum motor and system efficiency with different values of $T_{\rm pw}$ are virtually the same, which implies that this optimal ratio is independent of the tooth-pitch width.

D. Influence of Remanence B_r of PMs

Fig. 8 shows the variations of the motor efficiency with R_m/R_e for two values of B_r at $T_{\rm pw} = 0.04$ m with the other parameters being the same as stated in Section V-C. In this case, however, Somaloy 700 is used instead of Somaloy 500. It can be seen that the system efficiency improves by $\sim$0.45% when B_r is increased from 1.04 to 1.14 T. It is also evident that the optimal ratio R_m/R_e for maximum motor efficiency decreases with the increase in B_r. This is due to that fact that a larger B_r produces stronger magnetic field, which makes it possible to increase the electrical load by decreasing the magnet radius to achieve a higher efficiency. The optimal ratio of R_m/R_e with $B_r = 1.14$ T and Somaloy 700 is again 0.4, which yields the maximum motor efficiency of 0.95.

It should be noted that the foregoing optimization does not take into account the eddy-current loss in the moving-magnet armature. This eddy-current loss, however, can be effectively reduced by circumferential segmentation of both the magnets and the back iron [23] and, therefore, has insignificant influence on the optimization. Nevertheless, it slightly reduces the achievable efficiency.

VI. Experimental Results

Based on the outcome of the design optimization, a prototype motor, whose design parameters are given in Table II, has been constructed. The sintered NdFeB magnets with $B_r = 1.04$ T are mounted on a mild-steel tube, whereas the SMC stator

TABLE II
Design Parameters of Short-Stroke Single-Phase Tubular PM Motor (M)

R_e	0.05	T_p	0.025	T_{pw}	0.04
R_m	0.02	T_{mr}	0.016	T_w	0.0095
G	0.0008	T_{mz}	0.009	b_0	0.008
h_m	0.004	h_{ys}	0.005	h_{ym}	0.0036

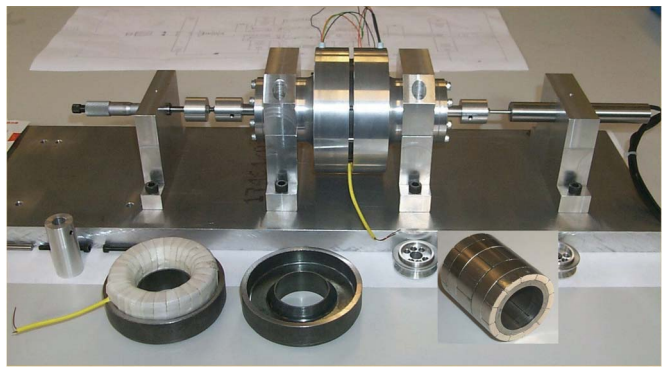

Fig. 9. Prototype tubular motor and static test rig.

core is manufactured from Somaloy 700. It should be noted that a lower value, 0.004 m, for the magnet thickness h_m was chosen to reduce the moving mass and to improve the dynamic capability of the compressor system [19]. This leads to a reduction in efficiency by $\sim$0.3%.

Fig. 9 shows the prototype motor mounted on a test rig with the excitation coils, the two identical SMC parts which form the stator core, and the moving-magnet armature with quasi-Halbach magnetized sintered NdFeB magnets. The variation of the thrust force of the prototype motor as a function of the armature displacement was measured by a force transducer mounted between a micrometer barrel, shown on the left of the test rig, and the motor shaft. The armature displacement was adjusted by the micrometer barrel and measured by a linear variable differential transformer, mounted on the right of the rig. To obtain the net thrust force, the variation of the cogging force with the armature position was first measured with the motor on an open circuit. The measurements were then repeated for different values of excitation current. The net thrust for a given current and armature displacement was then obtained by subtracting the measured cogging force from the total force. Fig. 10 compares the variation of the FE-predicted and measured thrust force for an excitation current of 1.0 A.

The efficiency of the motor is evaluated by the experimental setup shown in Fig. 11, where the two identical motors are connected back-to-back, one operating as a motor and the other as a generator whose output is connected to a variable resistor. Mechanical springs to facilitate resonant operation are incorporated in both machines.

The motor is supplied by a variable frequency/amplitude sinusoidal power source, and the input and output powers of the motor and generator are measured by the power analyzer. The losses of the machine under testing include the mechanical loss $P_{\rm ml}$ and the electromagnetic loss $P_{\rm el}$. The mechanical loss is due to the bearing friction and vibration of the test rig, and

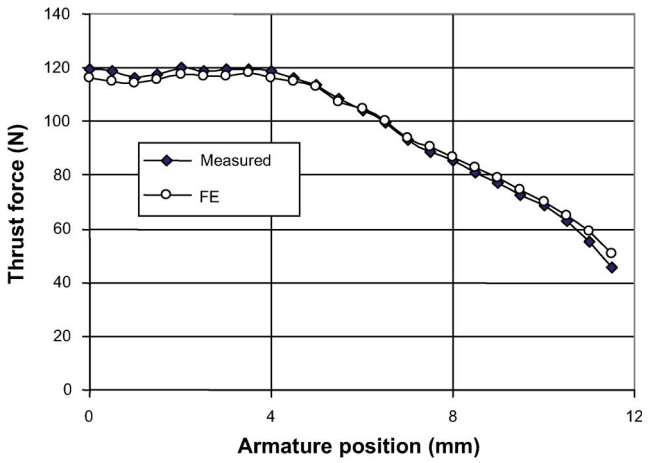

Fig. 10. Variation of measured and predicted thrust force with armature displacement for an excitation current of 1.0 A.

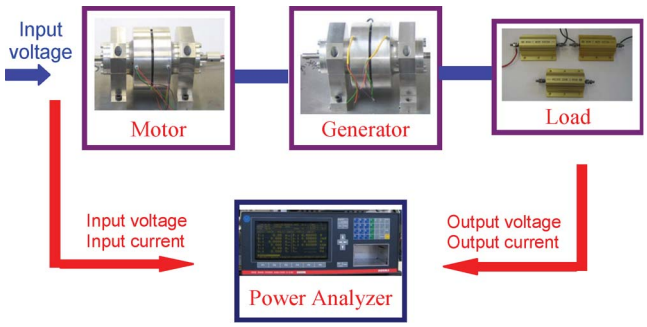

Fig. 11. Schematic of load-test setup for prototype motor.

the electromagnetic loss consists of the copper loss $P_{\rm cu}$, the iron loss $P_{\rm iron}$, and the eddy-current loss $P_{\rm eddy}$ of the moving-magnet armature. The sum of $P_{\rm iron}$ and $P_{\rm eddy}$ is denoted by $P_{\rm ie}$. To separate these loss components, three no-load tests were performed at a given supply frequency and armature stroke. The first no-load test was carried out with one motor only, and the total loss measured as the input power P_{L1} is given by

$$P_{L1} = P_{\rm ml} + P_{\rm ie} + P_{\rm cu1}. \tag{15}$$

The second no-load test was performed with two back-to-back connected machines, but the magnetic armature of the second machine was replaced by a dummy one with the same weight. Thus, the loss in the second machine is purely mechanical. Assume that the mechanical losses of the two machines are identical, the total no-load loss is given by

$$P_{L2} = 2P_{\rm ml} + P_{\rm ie} + P_{\rm cu2}. \tag{16}$$

In the third no-load test, the second machine is equipped with the magnetic armature which results in iron and eddy-current losses. Again, assume that these two loss components are identical in the two machines, the total no-load loss is given by

$$P_{L3} = 2P_{\rm ml} + 2P_{\rm ie} + P_{\rm cu3}. \tag{17}$$

The copper loss in each test can be quantified by measuring the input current and the coil resistance. Hence, the mechanical loss and the sum of the iron and eddy-current losses can be evaluated by

$$\begin{aligned} P_{\rm ml} &= (P_{L2} - P_{\rm cu2}) - (P_{L1} - P_{\rm cu1}) \\ P_{\rm ie} &= (P_{L3} - P_{\rm cu3}) - (P_{L2} - P_{\rm cu2}). \end{aligned} \tag{18}$$

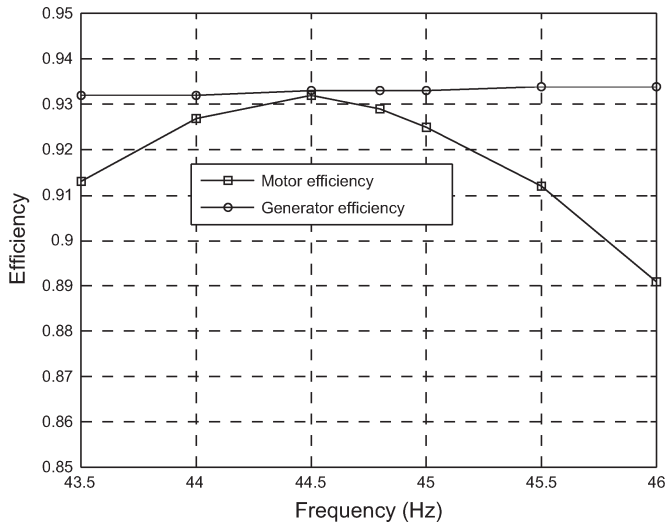

Fig. 12. Measured motor and generator efficiencies as functions of frequency at 10.0-mm stroke.

The variations of these two loss components as functions of supply frequency and armature stroke can be obtained by performing tests at different frequencies and strokes.

Load tests were performed on the back-to-back connected motor–generator system. The mechanical loss of the system can be separated from the measured input and output powers using the data obtained in the no-load tests. The copper loss of each machine is calculated from the measured current and coil resistance, and the efficiencies of the motor and generator are evaluated by the measured input and output powers and the iron-loss components obtained in the no-load tests. Fig. 12 shows the variation of the machine efficiencies with supply frequency for a fixed stroke of 10.0 mm when the generator was connected to a 440-Ω resistive load, and its output power varies from 72 to 80 W.

The resonant frequency of the system is 44.5 Hz when the equivalent stiffness of compressed gas is not present. As will be seen, the efficiency of the generator is above 93%, which is very close to the predicted value of 94%. The motor efficiency varies, however, from 89% to 93% since the system is not operating in resonance, and the stator current is much greater and the copper loss is higher, resulting in a lower efficiency.

VII. Conclusion

A design methodology to achieve optimal performance of the direct-drive linear compressor system employing a single-phase tubular PM motor has been described, and the influence of the leading design parameters on the system efficiency has been studied. It has been shown that in such a direct-drive system, the compressed gas has a significant effect on the input impedance of the electrical system, and it is essential

that the gas-load effect is taken into account in the design optimization. Experimental results have validated the proposed design methodology.

REFERENCES

[1] K. Park, E. P. Hong, and K. H. Lee, "Development of a linear motor for compressors of household refrigerators," in *Proc. LDIA*, Nagano, Japan, 2001, pp. 283–286.

[2] M. Utsuno, M. Takai, T. Yaegashi, T. Mizuno, H. Yamamoto, K. Shibuya, and H. Yamada, "Efficiency characteristics of a linear oscillatory actuator under simulated compressor load," in *Proc. LDIA*, Nagano, Japan, 2001, pp. 264–267.

[3] T. Chun, J. Ahn, J. Yoo, and C. Lee, "Analysis and control for linear compressor system driven by PWM inverter," in *Proc. 30th Annu. Conf. IEEE Ind. Electron. Soc.*, Busan, Korea, Nov. 2004, pp. 263–267.

[4] T.-W. Chun, J.-R. Ahn, H.-H. Lee, H.-G. Kim, and E.-C. Nho, "A novel strategy of efficiency control for a linear compressor system driven by a PWM inverter," *IEEE Trans. Ind. Electron.*, vol. 55, no. 1, pp. 296–301, Jan. 2008.

[5] I. Boldea and S. A. Nasar, *Linear Motion Electromagnetic Devices*. New York: Taylor & Francis, 2001.

[6] J. Wang, D. Howe, and Z. Lin, "Comparative studies on linear motor topologies for reciprocating vapour compressors," in *Proc. IEMDC*, Antalya, Turkey, May 3–5, 2007, pp. 364–369.

[7] J. F. Eastham, "Novel synchronous machines: Linear and disc," *Proc. Inst. Elect. Eng.*, vol. B-137, no. 1, pp. 49–58, Jan. 1990.

[8] J. Wang, W. Wang, G. W. Jewell, and D. Howe, "A low power, linear, permanent-magnet generator/energy storage system," *IEEE Trans. Ind. Electron.*, vol. 49, no. 3, pp. 640–648, Jun. 2002.

[9] J. Hirai, T.-W. Kim, and A. Kawamura, "Position-sensorless drive of linear pulse motor for suppressing transient vibration," *IEEE Trans. Ind. Electron.*, vol. 47, no. 2, pp. 337–345, Apr. 2000.

[10] J. Batelaan, "A linear motor design provides close and secure vehicle separation of many transit vehicles on a guideway," *IEEE Trans. Ind. Electron.*, vol. 54, no. 3, pp. 1778–1782, Jun. 2007.

[11] N. Bianchi, S. Bolognani, D. D. Corte, and F. Tonel, "Tubular linear permanent magnet motors: An overall comparison," *IEEE Trans. Ind. Appl.*, vol. 39, no. 2, pp. 466–475, Mar./Apr. 2003.

[12] A. Canova, G. Gruosso, and M. Repetto, "Synthesis of linear actuators," *COMPEL*, vol. 20, no. 3, pp. 713–723, 2001.

[13] H. S. Lim and R. Krishnan, "Ropeless elevator with linear switched reluctance motor drive actuation systems," *IEEE Trans. Ind. Electron.*, vol. 54, no. 4, pp. 2209–2218, Aug. 2007.

[14] H. S. Lim, R. Krishnan, and N. S. Lobo, "Design and control of a linear propulsion system for an elevator using linear switched reluctance motor drives," *IEEE Trans. Ind. Electron.*, vol. 55, no. 2, pp. 534–542, Feb. 2008.

[15] J. Wang, G. W. Jewell, and D. Howe, "Design optimization and comparison of tubular permanent magnet machine topologies," *Proc. Inst. Elect. Eng.—Electr. Power Appl.*, vol. 148, no. 5, pp. 456–464, 2001.

[16] J. Wang, Z. Lin, and D. Howe, "Analysis of a short-stroke, single phase, quasi-Halbach magnetized tubular permanent magnet motor for linear compressor applications," *IET Electr. Power Appl.*, vol. 2, no. 3, pp. 193–200, May 2008.

[17] B. L. J. Gysen, E. A. Lomonova, J. J. H. Paulides, and A. J. A. Vandenput, "Analytical and numerical techniques for solving Laplace and Poisson equations in a tubular permanent-magnet actuator: Part I. Semi-analytical framework," *IEEE Trans. Magn.*, vol. 44, no. 7, pp. 1751–1760, Jul. 2008.

[18] N. Schofield, A. Canova, G. Gruosso, M. Repetto, and M. Ottella, "The application of soft magnetic composites to the design of tubular linear actuators," *Int. J. Appl. Electromagn. Mech.*, vol. 19, no. 1–4, pp. 225–229, 2004.

[19] G. S. Choe and K. J. Kim, "Analysis of non-linear dynamics in linear compressor," *JSME Int. J., Ser. C*, vol. 43, no. 3, pp. 545–552, 2000.

[20] J. Wang, Z. Lin, and D. Howe, "Characteristics of linear compressors under current source excitation," *Proc. Inst. Mech. Eng. A, J. Power Energy*, vol. 221, no. 7, pp. 1057–1065, 2007.

[21] G. Bertotti, A. Canova, M. Chiampi, D. Chiarabaglio, F. Fiorillo, and A. M. Rietto, "Core loss prediction combining physical models with numerical field analysis," *J. Magn. Magn. Mater.*, vol. 133, no. 1–3, pp. 647–650, May 1994.

[22] Hoganas, Somoloy brochure. [Online]. Available: www.Hoganas.com

[23] J. Chai, J. Wang, and D. Howe, "Evaluation of eddy current loss in tubular permanent magnet motors by three-dimensional finite element analysis," presented at the XVII Int. Conf. Electrical Machines (ICEM), Chania, Greece, Sep. 2–5, 2006, Paper PSA1-12.

Jiabin Wang (SM'03) received the B.Eng. and M.Eng. degrees in electrical and electronic engineering from Jiangsu University of Science and Technology, Zhengjiang, China, in 1982 and 1986, respectively, and the Ph.D. degree in electrical and electronic engineering from the University of East London, London, U.K., in 1996.

From 1986 to 1991, he was with the Department of Electrical Engineering, Jiangsu University of Science and Technology, where he was appointed a Lecturer in 1987 and an Associate Professor in 1990. He was a Postdoctoral Research Associate at The University of Sheffield, Sheffield, U.K., from 1996 to 1997 and a Senior Lecturer at the University of East London from 1998 to 2001. He is currently a Reader in electrical engineering in the Electrical Machines and Drives Research Group, Department of Electrical and Electronic Engineering, The University of Sheffield. His research interests range from motion control to electromagnetic devices and their associated drives in applications ranging from automotive and household appliances to aerospace sectors.

David Howe received the B.Tech. and M.Sc. degrees in electrical power engineering from the University of Bradford, Bradford, U.K., in 1966 and 1967, respectively, and the Ph.D. degree in electrical power engineering from the University of Southampton, Southampton, U.K.

He has held academic posts at Brunel University, London, U.K., and the University of Southampton, and spent a period in industry with NEI Parsons Ltd., Newcastle-Upon-Tyne, U.K., working on electromagnetic problems related to turbogenerators. He is currently Emeritus Professor of electrical engineering in the Department of Electrical and Electronic Engineering, The University of Sheffield, Sheffield, U.K., where he heads the Electrical Machines and Drives Research Group. His research activities span all facets of controlled electrical-drive systems with particular emphasis on permanent-magnet-excited machines.

Dr. Howe is a Fellow of the Institution of Engineering and Technology, U.K., and a Fellow of the Royal Academy of Engineering, U.K.

Zhengyu Lin (S'03–M'05) received the B.Sc. and M.Sc. degrees from Zhejiang University, Hangzhou, China, in 1998 and 2001, respectively, and the Ph.D. degree from Heriot-Watt University, Edinburgh, U.K., in 2005.

From August 2004 to June 2006, he was a Research Associate in the Department of Electronic and Electrical Engineering, The University of Sheffield, Sheffield, U.K. Since July 2006, he has been an R&D Engineer with Emerson Industrial Automation, Control Techniques PLC, Newtown, Powys, U.K. His research interests include power electronics and electrical motor controls.